Heat Flux Management via Advanced Magnetic Divertor Configurations and Divertor Detachment

E. Kolemen [a], S.L. Allen [b], B.D. Bray [c], M.E. Fenstermacher [b], D.A. Humphreys [c], A.W. Hyatt [c], C.J. Lasnier [b], A.W. Leonard [c], M.A. Makowski [b], A.G. McLean [b], R. Maingi [a], R. Nazikian [a], T.W. Petrie [c], V.A. Soukhanovskii [b], and E.A. Unterberg [d]

[a] *Princeton Plasma Physics Laboratory, P.O. Box 451, Princeton, NJ 08540, USA*
[b] *Lawrence Livermore National Laboratory, Livermore, California, USA*
[c] *General Atomics, P.O. Box 85608, San Diego, California 92186-5608, USA*
[d] *Oak Ridge National Laboratory, Oak Ridge, Tennessee, USA*

ekolemen@pppl.gov

The Snowflake Divertor (SD) control and detachment control to manage the heat flux at the divertor are successfully demonstrated at DIII-D. Results of the development and implementation of these two heat flux reduction control methods are presented.

1. Snowflake Divertor control

The present vision of the tokamak plasma–material interface is an axisymmetric magnetic X-point divertor. One approach to handling the high heat exhaust per unit area on the PFCs is to use alternative magnetic configurations. Examples of these advanced divertors are the snowflake divertor (SD), X-divertor, super X-divertor, and X-point target divertor. These configurations require active and precise control of the magnetic configuration in order to regulate the particle and heat flow.

Recent research at DIII-D focused on SD configuration, which uses a second-order poloidal field null created by merging, or bringing close to each other, two first-order poloidal field null points (X-points) of a standard divertor configuration. A poloidal cross-section of the obtained magnetic flux surfaces with a hexagonal null-point has the appearance of a snowflake. The SD geometry results in high poloidal flux expansion and a large plasma wetted area compared to the standard divertor, which reduces peak heat flux. Also, SD has four strike points which help share the divertor power load compared to the regular two strike point configuration.

The exact second-order null configuration is topologically unstable to variations in the plasma dynamics and coil currents. This destroys the perfect alignment and splits the double null into two first order null X-points. Two variants of the exact configuration called snowflake-plus and snowflake-minus are often realized in steady state, as shown in Figure 1.

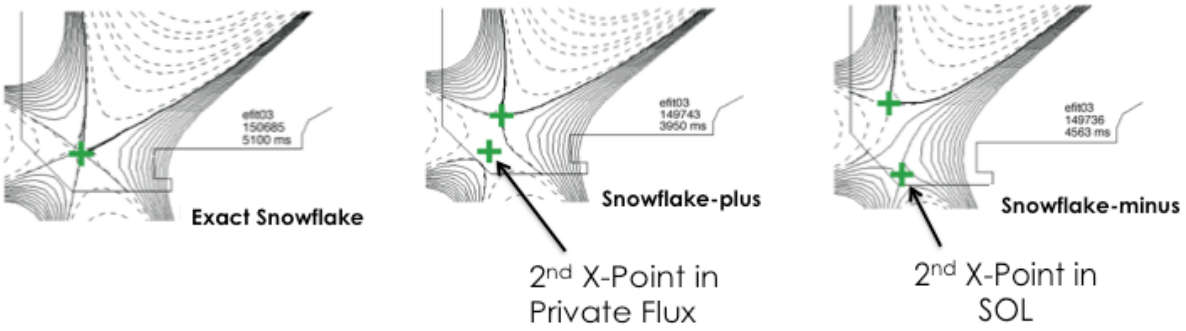

Figure 1. Three plasma equilibria in DIII-D showing the exact snowflake configuration with a double null, the snowflake-minus configuration with the secondary X-point in the private flux region, and the snowflake-plus configuration with the secondary X-point in the Scrap-Off Layer (SOL).

We implemented the world's first real-time SD detection and control system on DIII-D in order to stabilize this configuration. This control employs a fast real-time snowflake identification algorithm, which accurately calculates two X-points (magnetic nulls) by locally expanding the Grad-Shafranov equation in toroidal coordinates. We assume that the plasma in the divertor region has a low beta, and the magnetic field there can be considered curl-free. Then, the equations in toroidal coordinates around the divertor

$$(R+x)\frac{\partial}{\partial x}\left(\frac{1}{R+x}\frac{\partial \Psi}{\partial x}\right)+\frac{\partial^2 \Psi}{\partial z^2}=0$$

is normalized such that

$$\rho=\frac{x}{R}, \qquad \zeta=\frac{z-z_0}{R}$$

and Ψ is expanded in ρ and ζ up to the third order terms. Solving the first two orders of the expanded Grad-Shafranov equation gives us six unknown expansion coefficients. These unknowns are solved by, first, choosing three points around the snowflake center, and then evaluating the components of the magnetic field given as

$$B_\rho=-\frac{1}{1+\rho}\frac{\partial \Psi}{\partial \zeta}, \qquad B_\zeta=\frac{1}{1+\rho}\frac{\partial \Psi}{\partial \rho}$$

from the real-time equilibrium reconstruction (rt-EFIT). This gives us six linear equations for the six unknown expansion coefficients. These equations are solved using Gaussian elimination. Finally, we find the locations of the X-points, i.e. the magnetic field nulls, by solving the $B_\rho=0$, $B_\zeta=0$. This one step algorithm (no iteration is necessary) has been implemented in the DIII-D Plasma Control System (PCS), resulting in a fast execution time (<<1ms) with reasonable accuracy.

Once the locations of the two X-points are obtained, polodial field (PF) coils are used to control the relative locations to obtain the desired SD (exact, minus, plus). At DIII-D, the

F4B, F5B, F8B are the PF coils closest to the divertor, and they have thus been used to control the SD. F9B is also effective in the SD manipulation. However, plasma operation requires the avoidance of the strike point getting inside the cyropump gap under any possible circumstance to prevent damage to the unprotected cables and diagnostics inside the cyropump gap. To satisfy this constraint without inducing any hardware or software protection, we accepted to set the F9B coil to be zero current.

The SD control algorithm calculates the distance, angle, and r and z components of the relative positions of the two X-points in addition to the strike point locations. The values are compared to the user-requested values and the differences are filtered and fed to a Proportional-Integral-Derivative (PID) control algorithm. The eight control outputs of this PID control are then multiplied with a 3 by 8 matrix to obtain the PF coil voltage requests to the power supplies.

An example of an almost exact SD obtained with this control is shown in Figure 2, where the SD control is turned on at 3 seconds (shown with the red line) and ρ is controlled to a few cm until the end of the shot. Note that this is within the grid resolution of the rt-EFIT. Also, as the distance between the X-points becomes very small and almost exact SD is achieved, normal variations in the rt-EFIT reconstruction lead to large changes in the SD angle, which cannot be avoided. As the perfect SD is approached, broadening of the heat flux profile at the outer strike point is observed, as shown in Figure 3.

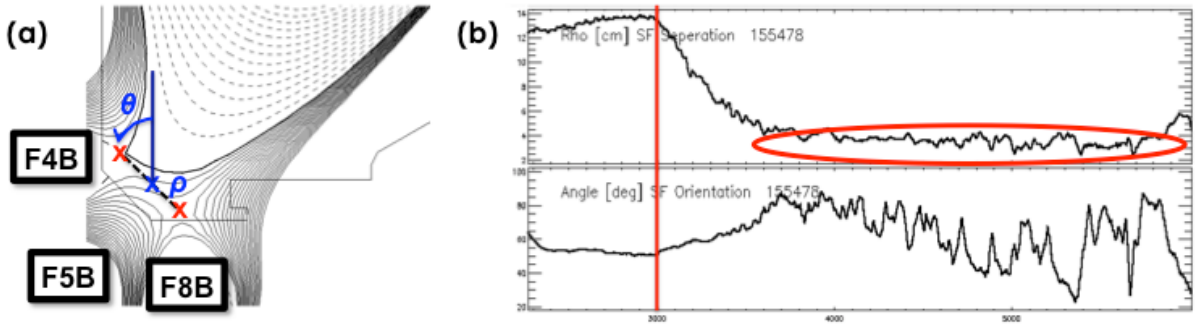

Figure 2. (a) PF coils used in SD control and the definition of the SD configuration parameters. (b) Plasma controlled to almost exact SD. The SD control starts at 3000 ms.

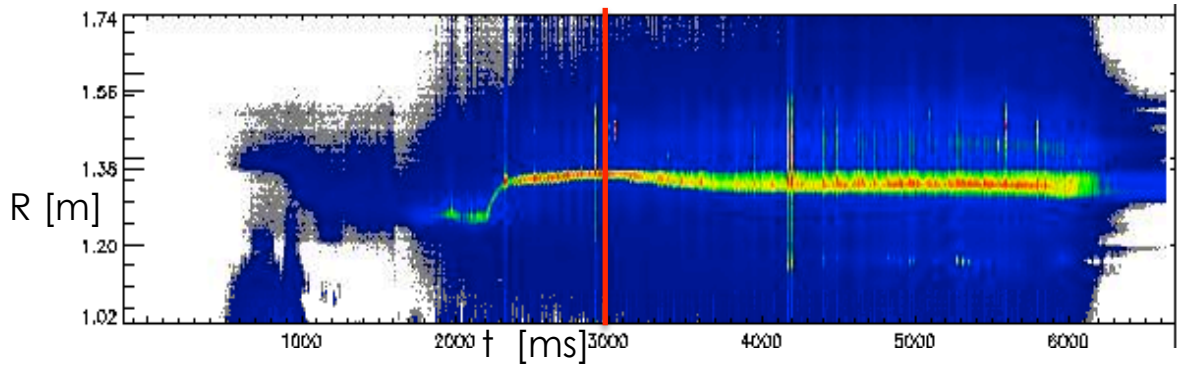

Figure 3. Broadening of the heat flux at the outer divertor for shot #155478.

This control enabled SD minus, SD plus and exact SD formations with varying σ, the distance between the X-points normalized to the minor radius, ranging from 0.08 to 0.5 in various scenarios. SD was successfully integrated to an advanced tokamak (AT) scenario with β_N = 3.0 and H98(y,2) ≅ 1.35. The flux profile for AT scenario with standard divertor and SD is shown in Figure 4. We achieved a 2.5 times increase in the flux expansion and a 2.5 reduction in peak heat flux for many energy confinement times (2-3 s) without any adverse effect to core plasma such as confinement. The maximum allowable heat flux on plasma-facing tiles stipulate that SD will operate under radiative conditions for fusion reactors. The radiative SD regime was explored with the gas seeding. SD control was shown to be robust under partial and full detachment conditions.

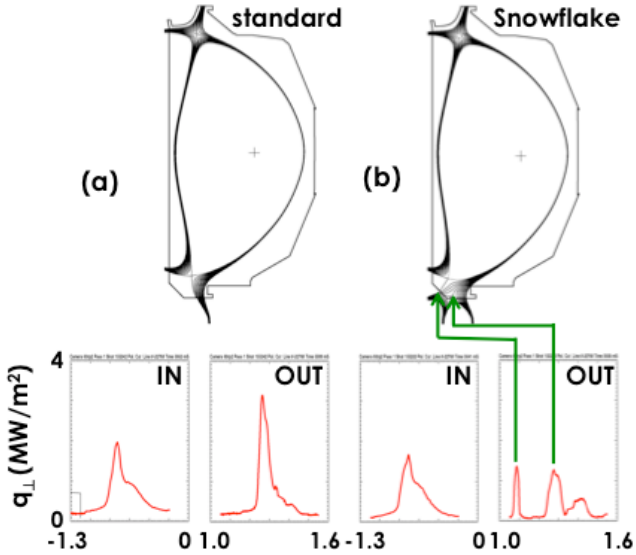

Figure 4. The heat flux profile at the inner and outer strike point for (a) the standard divertor double null AT and (b) the SD (-) double null AT.

2. Detachment control

Divertor "detachment" where the particle flux at the target plates drops by more than an order of magnitude is achieved by increasing the density close to the divertor. The ITER tokamak and future fusion reactors will require detached divertor plasmas to achieve acceptable divertor target heat loads. However, it is difficult to stabilize this effect when plasmas become fully detached. The influx of impurities into the confined plasma cause high radiation levels from this region, which may result in the thermal instability of the whole plasma, known as MARFE (Multi-faceted Asymmetric Radiation From the Edge). Thus, ITER needs to operate in a state called partial detachment under active feedback control in order to balance the need for acceptable divertor target heat loads and core stability.

We developed a new feedback control system on DIII-D to regulate and study the physics of divertor detachment. The system uses real-time electron temperature measurements from Thomson scattering, along with impurity line ratio measurement, to compute the location of the detachment front, while monitoring the core and divertor radiation measured by the bolometer diagnostic. We used the new system to test the feasibility of the envisioned ITER partial-detachment operation using divertor Thomson measurements on DIII-D. (ITER will

have a divertor Thomson with the diagnostic capability to measure as low as 1 eV.) This control regulates the detachment front while minimizing the effect of the detachment on the core by fixing the core density independent of the detachment control. This is achieved by a feedback control system that uses two gas valves as shown in Figure 5. The valve close to the strike point regulates both deuterium fuel and impurity gas injection rates to maintain the detachment front (where the plasma temperature drops to less than a few eV) at a pre-set distance from the divertor target using the real-time electron temperature measurements. The far-away valve keeps the core density stationary by using the interferometry measurements.

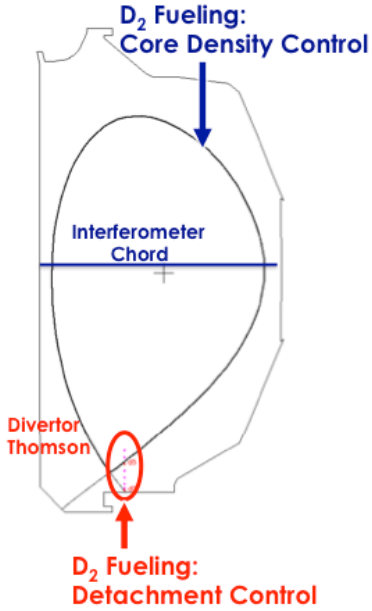

Figure 5. Sketch of the Partial-Detachment Control System

A comparison of two DIII-D L-mode shots with and without detachment controller is shown in Figure 6. This control stabilized the detachment front fixed at the mid distance between the strike point and the X-point throughout the shot, as shown in the 2D Thomson projection in Figure 7. This partial detachment reduces the radiation peak from the strike point and spreads it across the detached area, as shown in Figure 8. The new system allows systematic study of the physics of plasma detachment and plasma-surface interactions under constant, reproducible conditions. Data from these experiments will be used to test 2D models of the scrape-off layer and divertor plasma as well as to interpret surface erosion and material migration measurements.

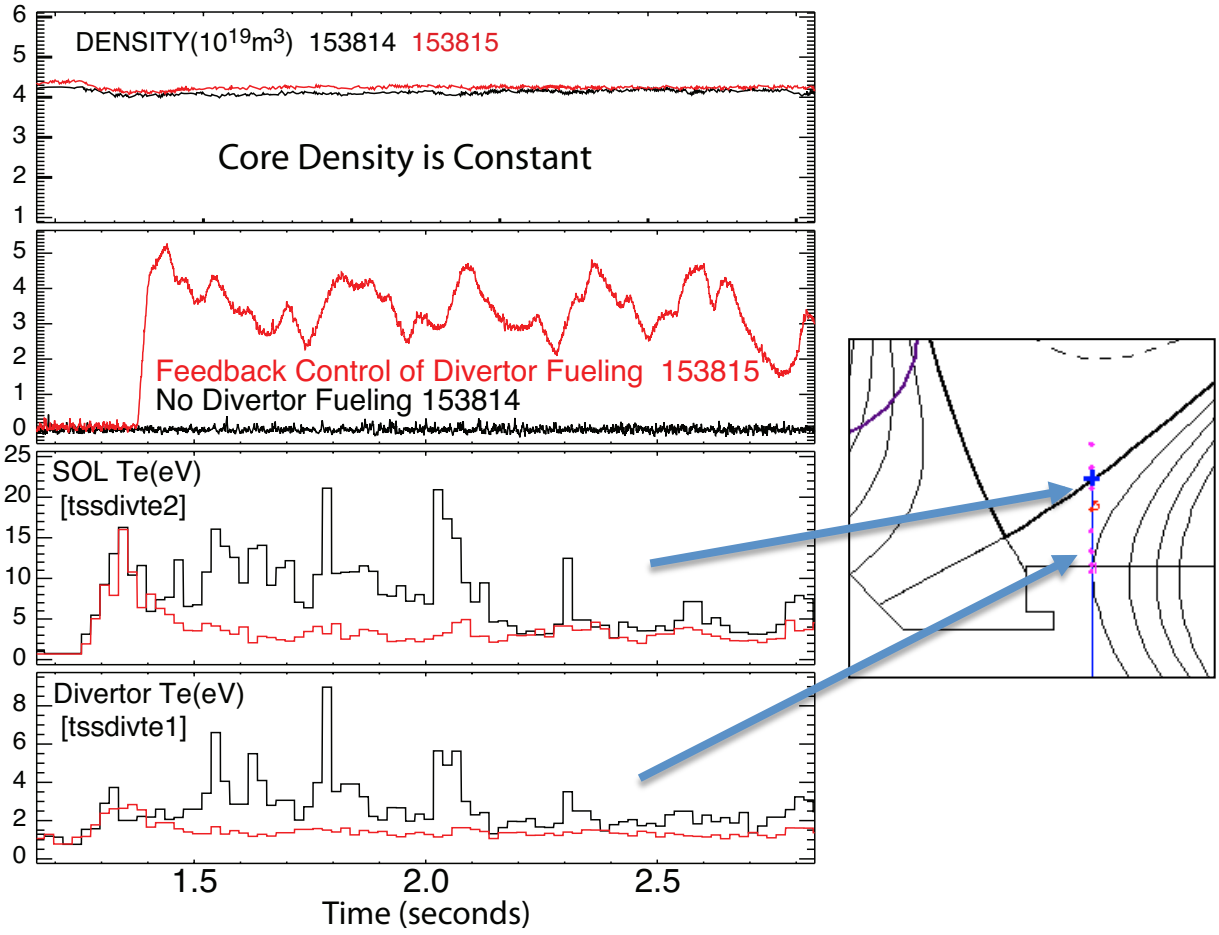

Figure 6. Data showing feedback control of divertor detachment. Red—detachment feedback control on. Black—detachment control off (no divertor fueling). Top: line average core density. Top-middle: Gas fueling rate. Bottom-middle: SOL electron temperature at ~20cm above divertor. Bottom: electron temperature just above divertor plate. Inset: divertor geometry.

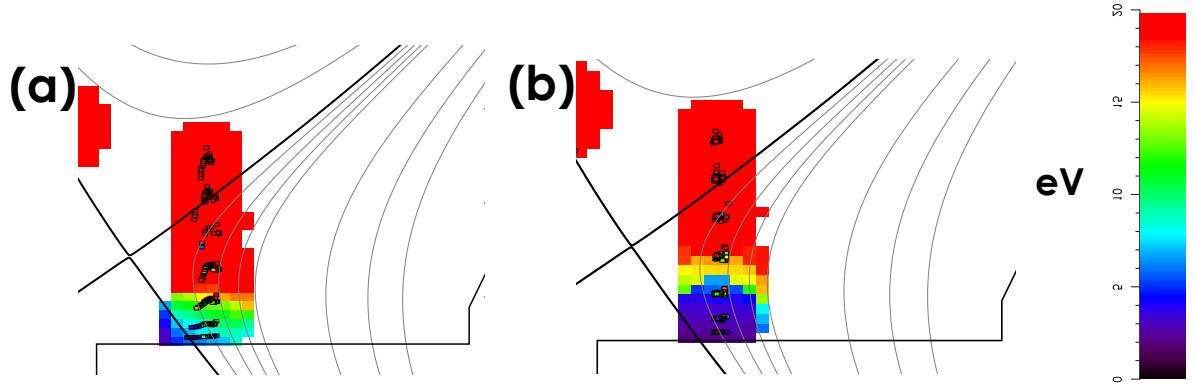

Figure 7. 2D Projected divertor Thomson temperature measurements for DIII-D: (a) shot without detachment control (#153814) shows no detachment, (b) shot with partial-detachment control (#153816) achieves detached cold front region shown in purple and blue.

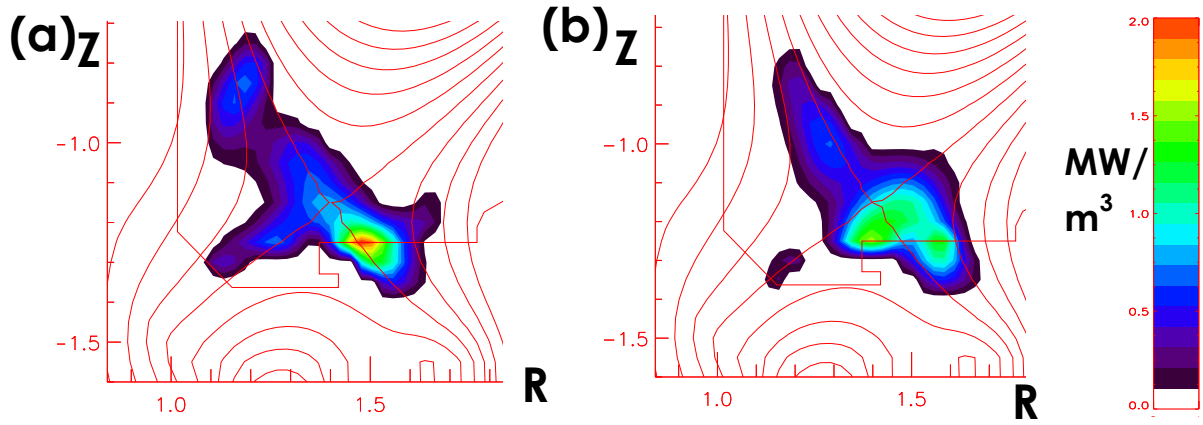

Figure 8. Radiation profile for DIII-D: (a) shot without detachment control (#153814) shows peaked radiation from the strike point, (b) shot with partial-detachment control (#153816) spreads the radiation across the detached area.